

Artificial topological insulator realized in a two-terminal Josephson junction with Rashba spin-orbit interaction

Luka Medic,^{*} Anton Ramšak, and Tomaž Rejec

Jožef Stefan Institute, Jamova 39, SI-1000 Ljubljana, Slovenia and

Faculty of Mathematics and Physics, University of Ljubljana, Jadranska 19, SI-1000 Ljubljana, Slovenia

(Dated: December 9, 2024)

We study a two-terminal Josephson junction with conventional superconductors and a normal region with Rashba spin-orbit interaction, characterized by two Aharonov-Casher (AC) fluxes. When the superconducting phase difference equals π , the Andreev subgap spectrum may host zero-energy Weyl singularities associated with a vanishing normal-state reflection eigenvalue. With one of the AC fluxes playing the role of a quasimomentum, the junction can be viewed as an artificial one-dimensional chiral topological insulator. Its topological phase can be tuned by crossing a Weyl singularity by means of varying the remaining AC flux. By associating an additional component of the quasimomentum with the superconducting phase difference, an artificial Chern insulator is realized.

Introduction.—The exploration of topology in condensed matter physics has flourished in recent decades [1–3]. Notably, Riwar et al. [4] introduced a novel class of topological systems by demonstrating that combining topologically trivial superconducting leads to form a multi-terminal Josephson junction may result in a topologically non-trivial system, an artificial topological material, where independent superconducting phase differences act as quasimomenta in a synthetic Brillouin zone (BZ). Central to their proposal were superconducting-phase-dependent Andreev bound states (ABSs), which could undergo a topological phase transition, leading to a change in the topological invariant, the Chern number. Consequently, the system exhibits quantization of the transconductance, which represents the current response in one terminal to the voltage applied to another. Eriksson et al. [5] numerically analyzed the same system and confirmed the quantization of the transconductance. Research was also done on three-terminal junctions in the presence of magnetic flux through the normal region [6, 7]. In these systems, the Aharonov-Bohm phase associated with the magnetic flux serves as the control parameter. Although experimental studies on multi-terminal Josephson junctions have been conducted [8–13], none have yet demonstrated the quantization of the transconductance.

In this Letter, similar to Ref. [6], we introduce a new control phase. Instead of the magnetic flux and the associated Aharonov-Bohm phase, we study systems exhibiting the spin-dependent Aharonov-Casher (AC) effect in the presence of the electric field [14–19]. In quasi-1D quantum wires, the AC phase can be induced by the Rashba spin-orbit coupling [20–23], where electrons with opposite spins acquire opposite phases [24–26]. For an InGaAs-based two-dimensional electron gas, the Rashba coupling, which can be controlled by a gate voltage, typically takes values in the range of $(0.5 - 2.0) \times 10^{-11}$ eVm [27–29]. In Rashba-gate-controlled rings [28–31], this corresponds to val-

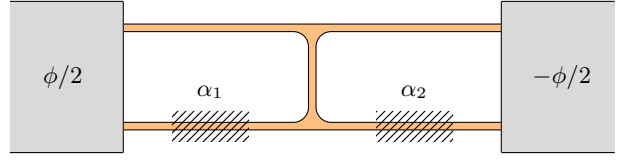


Figure 1. SNS Josephson junction with a superconducting phase difference ϕ and a normal region (orange) consisting of inter-connected quantum wires, forming two rings (genus 2). Each ring can be assigned an independent AC flux ($\alpha_{1,2}$), controllable via Rashba coupling using gate electrodes (hatched).

ues of the AC flux between 0.3π and 3π .

Studies on the effects of spin-orbit interaction in multi-terminal Josephson junctions have already been conducted [32, 33]. These investigations examined the ABS spectrum, including the impact of spin-orbit interaction on Weyl nodes and superconducting gap edge touchings. However, the consideration of spin-orbit phenomena as a new possibility for the quasimomentum of a synthetic BZ has not been explored in these works.

Here, we present a theoretical analysis focused on the exploration of low-dimensional, topologically non-trivial artificial materials utilizing the Rashba interaction within the normal region. The minimal model consists of a two-terminal Josephson junction with a normal region composed of two rings, as depicted in Fig. 1, each permeated by an AC flux. Our investigation concludes that both the winding number and the Chern number can be identified in this system. For the Chern number, the system’s synthetic BZ consists of an AC flux and the superconducting phase difference, whereas for the winding number, the superconducting phase difference is fixed to π .

The Letter is organized to first analyze the symmetries of a general multi-terminal system with multiple AC fluxes in the normal region and obtain the topological classification for this family of systems. Subsequently, we restrict ourselves to the analysis of systems with only two leads and two AC fluxes. The winding number is computed, and with the help of

^{*} luka.medic@ijs.si

the low-energy Hamiltonian at the Weyl node, its connection to the Chern number is established. Utilizing the system's symmetries, we conclude that for each spin sector, Weyl nodes come in quartets with pairs of opposite topological charges.

Symmetries.—We consider a general case of a multi-terminal Josephson junction in the presence of AC fluxes in the normal region. The parameters of our model encompass a vector $\vec{\phi}$ containing the independent superconducting phase differences, and a vector $\vec{\alpha}$ describing the AC fluxes through the normal region. Specifically, there is one AC flux for each ring (refer to Fig. 1).

We begin with the electron Hamiltonian, which describes the system in its normal state and has the following structure [28, 29]:

$$H(\vec{\alpha}) = \begin{bmatrix} H_{\uparrow}(\vec{\alpha}) & 0 \\ 0 & H_{\downarrow}(\vec{\alpha}) \end{bmatrix}. \quad (1)$$

Since electrons with opposite spins acquire opposite AC phases, the non-zero blocks satisfy the relations $H_{\downarrow}(\vec{\alpha}) = H_{\uparrow}(-\vec{\alpha}) = H_{\uparrow}(\vec{\alpha})^*$. Consequently, H exhibits symmetry under conjugation and time-reversal symmetry (TRS):

$$H(\vec{\alpha})^* = H(-\vec{\alpha}), \quad (2a)$$

$$TH(\vec{\alpha})T^{-1} = H(\vec{\alpha}), \quad (2b)$$

where $T = i\sigma_y\mathcal{K}$; here, σ_y is the Pauli matrix operating on the spin degree of freedom, and \mathcal{K} is the conjugation operator.

This allows us to represent the Bogoliubov-de Gennes (BdG) Hamiltonian, which incorporates the description of superconductivity, as

$$H_{\text{BdG}}(\vec{\phi}, \vec{\alpha}) = \begin{bmatrix} H(\vec{\alpha}) & \Delta(\vec{\phi}) \\ \Delta(\vec{\phi})^\dagger & -TH(\vec{\alpha})T^{-1} \end{bmatrix}, \quad (3)$$

where $\Delta(\vec{\phi})$ is a diagonal matrix for the s-wave pairing. In this form of the BdG Hamiltonian, the intrinsic particle-hole symmetry (PHS) is expressed as

$$\tau_y \sigma_y H_{\text{BdG}}^*(\vec{\alpha}, \vec{\phi}) \sigma_y \tau_y = -H_{\text{BdG}}(\vec{\alpha}, \vec{\phi}), \quad (4)$$

where τ_y is the Pauli matrix acting in the Nambu space. Additionally, from Eq. (2) and the relations $T\Delta(\vec{\phi})T^{-1} = \Delta(\vec{\phi})^* = \Delta(-\vec{\phi})$, it follows that the BdG Hamiltonian also exhibits symmetry under conjugation and TRS:

$$H_{\text{BdG}}^*(\vec{\alpha}, \vec{\phi}) = H_{\text{BdG}}(-\vec{\alpha}, -\vec{\phi}), \quad (5a)$$

$$\sigma_y H_{\text{BdG}}^*(\vec{\alpha}, \vec{\phi}) \sigma_y = H_{\text{BdG}}(\vec{\alpha}, -\vec{\phi}). \quad (5b)$$

The BdG Hamiltonian is symmetric under σ_z , i.e. $\sigma_z H_{\text{BdG}}(\vec{\alpha}, \vec{\phi}) \sigma_z = H_{\text{BdG}}(\vec{\alpha}, \vec{\phi})$, so the Hilbert space splits into two spin sectors. Hence, our focus lies on the classification within each sector. Combining Eqs. (4) and (5), we obtain two symmetries that do not mix the spin sectors:

$$\tau_y H_{\text{BdG}}^*(\vec{\alpha}, \vec{\phi}) \tau_y = -H_{\text{BdG}}(-\vec{\alpha}, \vec{\phi}), \quad (6a)$$

$$\tau_y H_{\text{BdG}}(\vec{\alpha}, \vec{\phi}) \tau_y = -H_{\text{BdG}}(\vec{\alpha}, -\vec{\phi}), \quad (6b)$$

$d_\alpha \backslash d_\phi$	0	1	2	3	4	5	6	7
0	0	0	\mathbb{Z}	\mathbb{Z}_2	\mathbb{Z}_2	0	$2\mathbb{Z}$	0
1	0	0	0	\mathbb{Z}	\mathbb{Z}_2	\mathbb{Z}_2	0	$2\mathbb{Z}$
2	$2\mathbb{Z}$	0	0	0	\mathbb{Z}	\mathbb{Z}_2	\mathbb{Z}_2	0
3	0	$2\mathbb{Z}$	0	0	0	\mathbb{Z}	\mathbb{Z}_2	\mathbb{Z}_2
4	\mathbb{Z}_2	0	$2\mathbb{Z}$	0	0	0	\mathbb{Z}	\mathbb{Z}_2
5	\mathbb{Z}_2	\mathbb{Z}_2	0	$2\mathbb{Z}$	0	0	0	\mathbb{Z}
6	\mathbb{Z}	\mathbb{Z}_2	\mathbb{Z}_2	0	$2\mathbb{Z}$	0	0	0
7	0	\mathbb{Z}	\mathbb{Z}_2	\mathbb{Z}_2	0	$2\mathbb{Z}$	0	0

Table I. Classification table for the case where the control parameter is a superconducting phase difference, resulting in the exclusive presence of PHS [Eq. (6a)] within each spin sector. Bott periodicity implies a periodic structure in d_ϕ and d_α with a period of 8.

which can be regarded as PHS and chiral symmetry (CS) within each sector. Note that, as a combination of TRS and the intrinsic PHS, chiral symmetry is generally preserved even in more complex Rashba interaction models.

Topological classification.—To transition a system between different topological phases, it is necessary to introduce at least one control parameter. Here, we focus on two scenarios: using either a single superconducting phase difference or a single AC flux as the control parameter. Selecting a superconducting phase difference as the control parameter breaks the CS described in Eq. (6b) while preserving the PHS described in Eq. (6a). Conversely, choosing an AC flux as the control parameter breaks the PHS while leaving the CS unaffected. Referring to Ref. [34], we have constructed topological classification tables for both scenarios (see Tables I and II); for specifics, refer to Supplemental Materials (SM) S1 [35]. In the tables, d_ϕ and d_α denote the dimensionalities of phases composing the synthetic BZ, culminating in its total dimensionality $d_{\text{BZ}} = d_\phi + d_\alpha$.

In Table I, the case [$d_\phi = 2, d_\alpha = 0$], having a topological invariant \mathbb{Z} , corresponds to the system with a non-trivial Chern number investigated in Ref. [4]. Specifically, the minimal model constitutes a four-terminal Josephson junction featuring three independent superconducting phases. Among these phases, two contribute to defining the synthetic BZ, while the remaining one functions as the control phase.

From here on, we restrict our analysis to systems with two superconducting leads only. In Table I, another consideration for identifying topologically non-trivial phases in low-dimensional systems is the option [$d_\phi = 0, d_\alpha = 2$]. In this case, the control parameter is the superconducting phase difference ϕ . Yet, as we will delve into in the subsequent sections, all the topological charges are situated at $\phi = \pi$ with a total charge of 0. Consequently, the behavior manifests as trivial.

Selecting one of the AC fluxes as the control parameter, Table II reveals that the lowest dimensional nontrivial cases are \mathbb{Z} and $\mathbb{Z} \oplus \mathbb{Z}$ for [$d_\phi = 0, d_\alpha = 1$] and [$d_\phi = 1, d_\alpha = 1$], respectively. Here, \mathbb{Z} represents the winding number, while $\mathbb{Z} \oplus \mathbb{Z}$ corresponds

d_α	even	odd
even	0	0
odd	\mathbb{Z}	$\mathbb{Z} \oplus \mathbb{Z}$

Table II. Classification table for the case where an AC flux is used as the control parameter, maintaining CS [Eq. (6b)] within each spin sector.

to the Chern number and the mirror winding number [34, 36, 37]. In the former case, the presence of CS requires the superconducting phase difference to be either 0 or π . Additionally, to allow for gap closures and enable topological phase transitions, we set $\phi = \pi$. Conversely, in the latter case, this constraint is lifted and ϕ is treated as a quasimomentum. For the remainder of the paper, our focus will be on these two cases, i.e. a two-terminal Josephson junction featuring two AC fluxes in the normal region.

Effective Hamiltonian.—We begin with the expression determining the Andreev bound states with energy E ($|E| < |\Delta|$) within the sector corresponding to electrons (holes) with spin \uparrow (\downarrow) [33, 38, 39]:

$$\begin{bmatrix} 0 & S_\uparrow(\vec{\alpha}) e^{i\hat{\phi}} \\ S_\downarrow^*(\vec{\alpha}) e^{-i\hat{\phi}} & 0 \end{bmatrix} \psi = e^{i\chi} \psi, \quad (7)$$

where $\chi \equiv \arccos(E/|\Delta|)$, with leads having the same gap $|\Delta|$. The components of $\psi = [\psi_e, \psi_h]^T$ are the amplitudes of the outgoing waves for electrons and holes. The matrix $\hat{\phi} = \text{diag}(\phi/2, -\phi/2) \otimes \mathbb{I}_N$ is diagonal, where $\phi \in [0, 2\pi)$ denotes the superconducting phase difference, and \mathbb{I}_N signifies the identity matrix with dimension N , indicating the number of modes in each lead. (We assume for simplicity that the number of modes in both leads is the same.) S_\uparrow (S_\downarrow^*) represents the normal-state scattering matrix for electrons (holes) with spin \uparrow (\downarrow); it is worth noting that $S_\downarrow(\vec{\alpha}) = S_\uparrow^T(\vec{\alpha})$. In the following, we will focus on the short junction limit, described by an energy-independent scattering matrix, and use the abbreviation $S = S_\uparrow(\vec{\alpha})$. A longer scattering region, characterized by an energy-dependent matrix $S(E)$, would lead to additional ABSs at finite energy. Nevertheless, the existence of Weyl nodes and their topological properties at zero energy depend solely on $S(0)$.

From Eq. (7), the equation for the electron part [40] can be obtained [4, 38]:

$$A\psi_e = e^{2i\chi}\psi_e, \quad (8)$$

where $A = S e^{i\hat{\phi}} S^\dagger e^{-i\hat{\phi}}$ is unitary. Similar to the Joukowski transform [41], we decompose $A = A_1 + iA_2$ into its hermitian and antihermitian component, where $A_1 = \frac{1}{2}(A + A^\dagger)$ and $A_2 = \frac{1}{2i}(A - A^\dagger)$ are both hermitian matrices. Separating the two parts of Eq. (8) yields a system of equations:

$$\left(\frac{\mathbb{I}_N - A_1}{2}\right)^{1/2} \psi_e = \sin \chi \psi_e, \quad (9a)$$

$$A_2 \psi_e = 2 \cos \chi \sin \chi \psi_e, \quad (9b)$$

where

$$\mathbb{I}_N - A_1 = 2 \sin^2 \frac{\phi}{2} \begin{bmatrix} t't^\dagger & 0 \\ 0 & tt^\dagger \end{bmatrix}, \quad (10a)$$

$$A_2 = 2 \sin \frac{\phi}{2} \begin{bmatrix} -t't^\dagger \cos \frac{\phi}{2} & rt^\dagger e^{i\frac{\phi}{2}} \\ tr^\dagger e^{-i\frac{\phi}{2}} & tt^\dagger \cos \frac{\phi}{2} \end{bmatrix}. \quad (10b)$$

Here, r (r') and t (t') are $N \times N$ reflection and transmission matrices at the left (right) lead, respectively, and $(\mathbb{I}_N - A_1)$ is positive semi-definite. In Eq. (9a), we took into account the constraint $\text{Im}(e^{i\chi}) \geq 0$ [38], i.e. $\chi \in [0, \pi]$. Assuming that $(\mathbb{I}_N - A_1)$ and A_2 are non-singular (requiring $\phi \neq 0$), we can combine Eqs. (9a) and (9b) to derive the effective (electron) Hamiltonian acting in the ABS subspace, $H_e \psi_e = E \psi_e$, given by

$$H_e = |\Delta| \begin{bmatrix} -(t't^\dagger)^{1/2} \cos \frac{\phi}{2} & rt^\dagger (tt^\dagger)^{-1/2} e^{i\phi/2} \\ (tt^\dagger)^{-1/2} tr^\dagger e^{-i\phi/2} & (tt^\dagger)^{1/2} \cos \frac{\phi}{2} \end{bmatrix}. \quad (11)$$

The eigenvalues of H_e come in pairs $E_n^\pm = \pm |\Delta| \sqrt{1 - T_n \sin^2(\phi/2)}$, where T_n are eigenvalues of tt^\dagger [38]. Thus, the gap closes when $\phi = \pi$ and $T_n = 1$. In the limit $\phi \rightarrow 0$, ABSs approach the continuum at $\pm |\Delta|$.

Chiral symmetry.—The chiral symmetry [Eq. (6b)] implies that eigenfunctions appear in pairs with opposite energies, satisfying $\Psi(\vec{\alpha}, -\vec{\phi}) = i\tau_y \Psi(\vec{\alpha}, \vec{\phi})$. This results in CS effectively swapping the roles of incoming and outgoing waves. Additionally, incoming waves are related to outgoing waves through Andreev reflection [38]. Consequently, under chiral symmetry, the components of outgoing waves (ψ_e, ψ_h) transform to $(e^{-i\hat{\phi}-i\chi}\psi_e, -e^{i\hat{\phi}-i\chi}\psi_h)$.

Focusing on the electron component, the effective Hamiltonian from the previous section satisfies $e^{i\hat{\phi}} H_e(\vec{\alpha}, 2\pi - \phi) e^{-i\hat{\phi}} = -H_e(\vec{\alpha}, \phi)$. For $\phi = \pi$, this reduces to $\Gamma_\pi H_e \Gamma_\pi^\dagger = -H_e$, where $\Gamma_\pi = \nu_z \otimes \mathbb{I}_N$ and ν_z is the Pauli matrix acting in the space of left and right outgoing waves. This is unsurprising, as H_e becomes block off-diagonal at $\phi = \pi$.

Topological invariants and the low-energy Hamiltonian.—We proceed by determining the topological invariant at $\phi = \pi$. From the topological classification, we already know that the appropriate invariant is the winding number [34, 42]. However, because the winding number is gauge-dependent, we will consider the differences between winding numbers at different values of the control AC flux. These differences correspond to contractible (i.e., null-homotopic) loops in the space of AC fluxes. For such loops, we derive:

$$W_\pi = \frac{1}{2\pi i} \oint_{C_\alpha} d \log(\det h) = \frac{1}{2\pi i} \oint_{C_\alpha} d \log(\det r), \quad (12)$$

where C_α is an arbitrary contractible loop, and $h = irt^\dagger (tt^\dagger)^{-1/2}$ is the off-diagonal block of H_e . In the last step, we assumed that C_α does not cross or enclose any gap edge touchings. Consequently, only the reflection matrix r contributes to W_π .

Next, let us focus on the low-energy limit, particularly on the band touching at a Weyl node located at $\vec{x}_w = [\alpha_{1w}, \alpha_{2w}, \pi]^T$. Denoting the two chiral states at the Weyl node with positive and negative chirality as $|a_e^+\rangle$ and $|a_e^-\rangle$, respectively (where $\nu_z|a_e^\pm\rangle = \pm|a_e^\pm\rangle$), we can express the low-energy Hamiltonian as (details in SM S2 [35])

$$H_w = \delta\vec{x} \cdot M_3 \vec{\Sigma}. \quad (13)$$

Here, $\delta\vec{x} = [\delta\alpha_1, \delta\alpha_2, \delta\phi]^T$ represents the displacement from the Weyl node, $\vec{\Sigma}$ is a vector of Pauli matrices acting in the space of chiral states $|a_e^\pm\rangle$, and

$$M_3 = \begin{bmatrix} M_2 & 0 \\ 0 & 0 & \frac{1}{2} \end{bmatrix}, \quad M_2 = \left[\begin{array}{cc} \partial_{\alpha_1} \text{Re}(\zeta) & -\partial_{\alpha_1} \text{Im}(\zeta) \\ \partial_{\alpha_2} \text{Re}(\zeta) & -\partial_{\alpha_2} \text{Im}(\zeta) \end{array} \right]_{\vec{x}=\vec{x}_w} \quad (14)$$

where $\zeta(\vec{x}) = \langle a_e^+ | H_e(\vec{x}) | a_e^- \rangle$, and M_2 is evaluated at the Weyl node. Thus, the low-energy dispersion at the Weyl node is conical, given by $E^\pm = \pm \sqrt{|\delta\vec{\alpha} \cdot \nabla_{\vec{\alpha}} \zeta|^2 + (\delta\phi/2)^2}$.

From Eq. (14), topological charges associated with winding and Chern numbers can be obtained as $W_w = \text{sgn}(\det(M_2))$ and $C_w = \text{sgn}(\det(M_3))$, respectively. It is clear that the two charges are equivalent, and we henceforth denote them as q_w .

Following the topological classification of the BdG Hamiltonian presented in Table II, the remaining invariant is the mirror winding number, defined as [36]

$$W_{MZ} = \text{sgn}(W_0 - W_\pi) (|W_0| - |W_\pi|), \quad (15)$$

where W_0 is the winding number evaluated in the plane $\phi = 0$. Although the winding number is well-defined for the entire BdG Hamiltonian, our approach involving scattering matrices and ABSs, which merge with the continuum, does not permit us to obtain W_0 in our present formulation. We leave the calculation of the mirror winding number of the BdG Hamiltonian for further study.

Applying conjugation symmetry, Eq. (5a), at the conjugation-invariant phase $\phi = \pi$ [43], leads us to the conclusion that Weyl nodes come in pairs at $\pm\vec{x}_w$ with equal topological charges, $q_w(\vec{x}_w) = q_w(-\vec{x}_w)$. Given this equivalence of topological charges and considering the Nielsen-Ninomiya theorem, which necessitates total charge cancellation [44–46], we infer the existence of quartets of Weyl nodes within each spin sector. Each quartet comprises of two Weyl nodes with positive topological charge and two with negative topological charge.

Considering both sectors, the TRS [Eq. (5b)] implies that $q_w^\downarrow(\vec{x}_w) = q_w^\uparrow(-\vec{x}_w) = q_w^\uparrow(\vec{x}_w)$, resulting in both sectors having identical topological charges at \vec{x}_w . Consequently, eigenstates at the Weyl nodes are topologically protected and can be gapped only by the annihilation of opposite charges. The total charge,

combining charges for both sectors, amounts to twice the topological charge for each individual sector.

Discussion.—To summarize, we provided a topological classification of multi-terminal Josephson junctions with AC fluxes in the normal region. In contrast to previous proposals for realizing Josephson junctions as topological matter [4, 6, 7], we showed that topologically non-trivial regimes can arise even in Josephson junctions with just two terminals. Specifically, for two-terminal Josephson junctions with the superconducting phase difference equal to π , we demonstrated that when no gap edge touchings are enclosed by C_α , the computation of winding number differences simplifies to the topological properties of the reflection matrix r . We confirmed that the dispersion near zero-energy singularities is conical, identifying these singularities as Weyl nodes. Additionally, we established the equivalence between the topological charges associated with the winding number and the Chern number. Finally, we showed that the Weyl nodes of the two spin sectors coincide and carry the same topological charges.

In our approach, we derived ABS spectra using scattering matrices. However, by neglecting the energy dependence of these matrices, we encountered ABS spectra with gap edge touchings. Incorporating energy dependence in the scattering matrix could introduce finite level repulsion between the highest ABS and the continuum, thereby restoring the adiabaticity of the ABSs, as discussed in Ref. [4]. Furthermore, as highlighted in the main text, another limitation of this scattering formalism and ABS-based approach is its inability to compute the mirror winding number of the BdG Hamiltonian. To address this, analytical generalizations similar to those proposed in Ref. [47] may be required.

Another challenge stems from the constrained variation range of the AC flux. To handle this limitation, a protocol should be devised that does not require quasimomentum variations exceeding 2π , unlike the protocol presented in Ref. [4]. The proposed protocol should identify a quantized physical observable related to either the winding number or the Chern number (or their associated topological charges). It is important to note that, unlike superconducting phases, which are associated with electric currents, AC fluxes are related to spin currents.

Further exploration of these ideas is a direction for future theoretical research. While we acknowledge that experimentally realizing the proposed systems remains challenging, we hope our results will inspire efforts toward the development of such devices.

We appreciate valuable discussions with Y. V. Nazarov and R. Žitko. The authors acknowledge support from the Slovenian Research and Innovation Agency (ARIS) under Contract No. P1-0044; AR was also supported by Grant J2-2514.

-
- [1] Ching-Kai Chiu, Jeffrey C. Y. Teo, Andreas P. Schnyder, and Shinsei Ryu, “Classification of topological quantum matter with symmetries,” *Rev. Mod. Phys.* **88**, 035005 (2016).
- [2] M. Z. Hasan and C. L. Kane, “Colloquium: Topological insulators,” *Rev. Mod. Phys.* **82**, 3045–3067 (2010).
- [3] Xiao-Liang Qi and Shou-Cheng Zhang, “Topological insulators and superconductors,” *Rev. Mod. Phys.* **83**, 1057–1110 (2011).
- [4] Roman-Pascal Riwar, Manuel Houzet, Julia S. Meyer, and Yuli V. Nazarov, “Multi-terminal Josephson junctions as topological matter,” *Nature Communications* **7**, 11167 (2016).
- [5] Erik Eriksson, Roman-Pascal Riwar, Manuel Houzet, Julia S. Meyer, and Yuli V. Nazarov, “Topological transconductance quantization in a four-terminal Josephson junction,” *Phys. Rev. B* **95**, 075417 (2017).
- [6] Julia S. Meyer and Manuel Houzet, “Nontrivial Chern Numbers in Three-Terminal Josephson Junctions,” *Phys. Rev. Lett.* **119**, 136807 (2017).
- [7] Hong-Yi Xie, Maxim G. Vavilov, and Alex Levchenko, “Topological Andreev bands in three-terminal Josephson junctions,” *Phys. Rev. B* **96**, 161406 (2017).
- [8] A. H. Pfeffer, J. E. Duvauchelle, H. Courtois, R. Mélin, D. Feinberg, and F. Lefloch, “Subgap structure in the conductance of a three-terminal Josephson junction,” *Phys. Rev. B* **90**, 075401 (2014).
- [9] E. Strambini, S. D’Ambrosio, F. Vischi, F. S. Bergeret, Yu. V. Nazarov, and F. Giazotto, “The ω -SQUIPT as a tool to phase-engineer Josephson topological materials,” *Nature Nanotechnology* **11**, 1055–1059 (2016).
- [10] Yonatan Cohen, Yuval Ronen, Jung-Hyun Kang, Moty Heiblum, Denis Feinberg, Régis Mélin, and Hadas Shtrikman, “Nonlocal supercurrent of quartets in a three-terminal Josephson junction,” *PNAS* **115**, 6991–6994 (2018).
- [11] Anne W. Draelos, Ming-Tso Wei, Andrew Seredinski, Hengming Li, Yash Mehta, Kenji Watanabe, Takashi Taniguchi, Ivan V. Borzenets, François Amet, and Gleb Finkelstein, “Supercurrent Flow in Multiterminal Graphene Josephson Junctions,” *Nano Letters* **19**, 1039–1043 (2019).
- [12] Gino V. Graziano, Joon Sue Lee, Mihir Pendharkar, Chris J. Palmström, and Vlad S. Pribiag, “Transport studies in a gate-tunable three-terminal Josephson junction,” *Phys. Rev. B* **101**, 054510 (2020).
- [13] Natalia Pankratova, Hanho Lee, Roman Kuzmin, Kaushini Wickramasinghe, William Mayer, Joseph Yuan, Maxim G. Vavilov, Javad Shabani, and Vladimir E. Manucharyan, “Multiterminal Josephson Effect,” *Phys. Rev. X* **10**, 031051 (2020).
- [14] Y. Aharonov and A. Casher, “Topological Quantum Effects for Neutral Particles,” *Phys. Rev. Lett.* **53**, 319–321 (1984).
- [15] A. Cimmino, G. I. Opat, A. G. Klein, H. Kaiser, S. A. Werner, M. Arif, and R. Clothier, “Observation of the topological Aharonov-Casher phase shift by neutron interferometry,” *Phys. Rev. Lett.* **63**, 380–383 (1989).
- [16] Harsh Mathur and A. Douglas Stone, “Quantum transport and the electronic Aharonov-Casher effect,” *Phys. Rev. Lett.* **68**, 2964–2967 (1992).
- [17] M. König, A. Tschetschetkin, E. M. Hankiewicz, Jairo Sinova, V. Hock, V. Daumer, M. Schäfer, C. R. Becker, H. Buhmann, and L. W. Molenkamp, “Direct Observation of the Aharonov-Casher Phase,” *Phys. Rev. Lett.* **96**, 076804 (2006).
- [18] Tobias Bergsten, Toshiyuki Kobayashi, Yoshiaki Sekine, and Junsaku Nitta, “Experimental Demonstration of the Time Reversal Aharonov-Casher Effect,” *Phys. Rev. Lett.* **97**, 196803 (2006).
- [19] Xin Liu, M. F. Borunda, Xiong-Jun Liu, and Jairo Sinova, “Control of Josephson current by Aharonov-Casher phase in a Rashba ring,” *Phys. Rev. B* **80**, 174524 (2009).
- [20] E. I. Rashba, “Symmetry of Energy Bands in Crystals of Wurtzite Type II. Symmetry of Bands with Spin-Orbit Interaction Included,” *Fiz. Tverd. Tela: Collected Papers* **2**, 62–76 (1959).
- [21] Yu. A. Bychkov and E. I. Rashba, “Properties of a 2D electron gas with lifted spectral degeneracy,” *JETP Letters* **39**, 66 (1984).
- [22] Yu A Bychkov and E I Rashba, “Oscillatory effects and the magnetic susceptibility of carriers in inversion layers,” *Journal of Physics C: Solid State Physics* **17**, 6039 (1984).
- [23] G Bihlmayer, O Rader, and R Winkler, “Focus on the Rashba effect,” *New Journal of Physics* **17**, 050202 (2015).
- [24] A. Manchon, H. C. Koo, J. Nitta, S. M. Frolov, and R. A. Duine, “New perspectives for Rashba spin-orbit coupling,” *Nature Materials* **14**, 871–882 (2015).
- [25] Damian Tomaszewski, Piotr Busz, Rosa López, Rok Žitko, Minchul Lee, and Jan Martinek, “Aharonov-Bohm and Aharonov-Casher effects for local and non-local Cooper pairs,” *Phys. Rev. B* **97**, 214506 (2018).
- [26] Damian Tomaszewski, Piotr Busz, Rosa López, Rok Žitko, Minchul Lee, and Jan Martinek, “Aharonov-Bohm and Aharonov-Casher effects in a double quantum dot Josephson junction,” *Phys. Rev. B* **98**, 174504 (2018).
- [27] Dirk Grundler, “Large Rashba Splitting in InAs Quantum Wells due to Electron Wave Function Penetration into the Barrier Layers,” *Phys. Rev. Lett.* **84**, 6074–6077 (2000).
- [28] R. Citro and F. Romeo, “Pumping in a mesoscopic ring with Aharonov-Casher effect,” *Phys. Rev. B* **73**, 233304 (2006).
- [29] B. H. Wu and J. C. Cao, “Analysis of spin pumping in asymmetric ring conductors with the Aharonov-Casher effect,” *Phys. Rev. B* **75**, 113303 (2007).
- [30] F. Romeo, R. Citro, and M. Marinaro, “Quantum pumping and rectification effects in Aharonov-Bohm-Casher ring-dot systems,” *Phys. Rev. B* **78**, 245309 (2008).
- [31] Matisse Wei-Yuan Tu, Amnon Aharony, Wei-Min Zhang, and Ora Entin-Wohlman, “Real-time dynamics of spin-dependent transport through a double-quantum-dot Aharonov-Bohm interferometer with spin-orbit interaction,” *Phys. Rev. B* **90**, 165422 (2014).
- [32] B. Béri, J. H. Bardarson, and C. W. J. Beenakker, “Splitting of Andreev levels in a Josephson junction by spin-orbit coupling,”

- [Phys. Rev. B **77**, 045311 \(2008\)](#).
- [33] Tomohiro Yokoyama and Yuli V. Nazarov, “Singularities in the Andreev spectrum of a multiterminal Josephson junction,” [Phys. Rev. B **92**, 155437 \(2015\)](#).
- [34] Ken Shiozaki and Masatoshi Sato, “Topology of crystalline insulators and superconductors,” [Phys. Rev. B **90**, 165114 \(2014\)](#).
- [35] See Supplemental Material for details on topological classification and an alternative approach utilizing the full Nambu space.
- [36] Ching-Kai Chiu, Hong Yao, and Shinsei Ryu, “Classification of topological insulators and superconductors in the presence of reflection symmetry,” [Phys. Rev. B **88**, 075142 \(2013\)](#).
- [37] Fan Zhang and C. L. Kane, “Anomalous topological pumps and fractional Josephson effects,” [Phys. Rev. B **90**, 020501 \(2014\)](#).
- [38] C. W. J. Beenakker, “Universal limit of critical-current fluctuations in mesoscopic Josephson junctions,” [Phys. Rev. Lett. **67**, 3836–3839 \(1991\)](#).
- [39] Yuli V. Nazarov and Yaroslav M. Blanter, *Quantum Transport: Introduction to Nanoscience* (Cambridge University Press, 2009).
- [40] In Supplemental Materials S2 [35], we present an alternative approach that considers both the electron and hole parts simultaneously. We demonstrate that the conclusions remain consistent with those obtained using the approach presented in this paper, which considered only the electron part when computing the effective Hamiltonian and the topological invariants.
- [41] B. van Heck, S. Mi, and A. R. Akhmerov, “Single fermion manipulation via superconducting phase differences in multiterminal Josephson junctions,” [Phys. Rev. B **90**, 155450 \(2014\)](#).
- [42] Maria Maffei, Alexandre Dauphin, Filippo Cerdano, Maciej Lewenstein, and Pietro Massignan, “Topological characterization of chiral models through their long time dynamics,” [New Journal of Physics **20**, 013023 \(2018\)](#).
- [43] Here, the conjugation symmetry, Eq. (5a), mimics TRS within each distinct sector, where $\phi = \pi$ is analogous to time-reversal invariant momentum (TRIM).
- [44] H.B. Nielsen and M. Ninomiya, “Absence of neutrinos on a lattice: (I). Proof by homotopy theory,” [Nuclear Physics B **185**, 20–40 \(1981\)](#).
- [45] H.B. Nielsen and M. Ninomiya, “Absence of neutrinos on a lattice: (II). Intuitive topological proof,” [Nuclear Physics B **193**, 173–194 \(1981\)](#).
- [46] Shuichi Murakami, “Phase transition between the quantum spin Hall and insulator phases in 3D: emergence of a topological gapless phase,” [New Journal of Physics **9**, 356 \(2007\)](#).
- [47] E. V. Repin, Y. Chen, and Y. V. Nazarov, “Topological properties of multiterminal superconducting nanostructures: Effect of a continuous spectrum,” [Phys. Rev. B **99**, 165414 \(2019\)](#).

Supplemental Materials

Artificial topological insulator realized in a two-terminal Josephson junction with Rashba spin-orbit interaction

Luka Medic,* Anton Ramšak, and Tomaž Rejec

Jožef Stefan Institute, Jamova 39, SI-1000 Ljubljana, Slovenia and

Faculty of Mathematics and Physics, University of Ljubljana, Jadranska 19, SI-1000 Ljubljana, Slovenia

(Dated: December 9, 2024)

S1. TOPOLOGICAL CLASSIFICATION USING K-THEORY

We regard the PHS symmetry [Eq. (4a) of the main text] as an additional anti-symmetric anti-unitary symmetry within class A of the standard Altland-Zirnbauer (AZ) periodic table. Following the K-theory framework outlined in Ref. [1], we derive

$$\begin{aligned} K_{\mathbb{C}}^A(s=6; d=d_\phi+d_\alpha, d_\parallel=d_\phi, D=0, D_\parallel=0) \\ = K_{\mathbb{C}}^A(6+d_\phi-d_\alpha; 0, 0, 0, 0) \\ = \pi_0(\mathcal{R}_{6+d_\phi-d_\alpha}) \end{aligned} \quad (1)$$

where Bott periodicity implies $\mathcal{R}_p \simeq \mathcal{R}_{p+8}$, π_0 is the 0th homotopy ‘group’, and \mathcal{R} represents the classifying space of real AZ classes. From Eq. (1) the Table I of the main text follows.

Similarly, the chiral symmetry [Eq. (4b) of the main text] is regarded as an additional unitary anti-symmetry within class A. This leads to the following expression:

$$\begin{aligned} K_{\mathbb{C}}^A(s=0, t=1; d=d_\phi+d_\alpha, d_\parallel=d_\phi, D=0, D_\parallel=0) \\ = K_{\mathbb{C}}^A(0-d_\phi-d_\alpha, 1-d_\phi; 0, 0, 0, 0). \end{aligned} \quad (2)$$

If d_ϕ is odd, Eq. (2) reduces to

$$\pi_0(\mathcal{C}_{-d_\phi-d_\alpha}) \oplus \pi_0(\mathcal{C}_{-d_\phi-d_\alpha}), \quad (3)$$

otherwise

$$\pi_0(\mathcal{C}_{1-d_\phi-d_\alpha}), \quad (4)$$

where \mathcal{C} represents the classifying space of complex AZ classes, and due to Bott periodicity we have $\mathcal{C}_p \simeq \mathcal{C}_{p+2}$. Knowing that $\pi_0(\mathcal{C}_0) = \mathbb{Z}$ and $\pi_0(\mathcal{C}_1) = 0$, Table II of the main text is obtained.

S2. ALTERNATIVE APPROACH UTILIZING THE FULL NAMBU SPACE

Below, we provide an alternative approach to obtain the effective ABS Hamiltonian. Instead of considering only the electron part as in the main text, we include the hole part as well. After deriving the effective Hamiltonian, we rewrite the chiral symmetry in the basis of outgoing waves. Following this, we compute the winding number and the low-energy two-level Hamiltonian. We show that this approach yields results identical to those presented in the main text, where only the electron part was considered.

A. Effective Hamiltonian

By the means of polar decomposition of the scattering matrix S [2, 3], let us transform the Eq. (5) of the main text. Polar decomposition of the scattering matrix S can be written as

$$S = V\tilde{S}U^\dagger \quad (5)$$

* luka.medic@ijs.si

where V and U are block diagonal unitary matrices

$$V = \begin{bmatrix} V_1 & 0 \\ 0 & V_2 \end{bmatrix}, \quad U = \begin{bmatrix} U_1 & 0 \\ 0 & U_2 \end{bmatrix}, \quad (6)$$

and

$$\tilde{S} = \begin{bmatrix} -i\sqrt{\mathcal{R}} & \sqrt{\mathcal{T}} \\ \sqrt{\mathcal{T}} & -i\sqrt{\mathcal{R}} \end{bmatrix}. \quad (7)$$

Here, $\mathcal{R} = \text{diag}(\mathcal{R}_n)$ and $\mathcal{T} = \mathbb{I}_N - \mathcal{R}$ are diagonal matrices, consisting of singular values of rr^\dagger and tt^\dagger , respectively. Now let us write a unitary transformation that does not mix electron and hole parts of the wavefunction:

$$\mathcal{U} = \begin{bmatrix} \mathcal{H}_{2N} e^{-i\hat{\phi}/2} V^\dagger & 0 \\ 0 & \mathcal{H}_{2N} e^{i\hat{\phi}/2} U^\dagger \end{bmatrix}, \quad (8)$$

where \mathcal{H}_{2N} represents the Hadamard matrix tensored with \mathbb{I}_N :

$$\mathcal{H}_{2N} = \frac{1}{\sqrt{2}} \begin{bmatrix} 1 & 1 \\ 1 & -1 \end{bmatrix} \otimes \mathbb{I}_N. \quad (9)$$

Note that $e^{i\hat{\phi}/2} = \text{diag}(e^{i\phi/4}, e^{-i\phi/4}) \otimes \mathbb{I}_N$ commutes with V and U . \mathcal{U} transforms Eq. (5) of the main text to

$$\begin{bmatrix} 0 & S' \\ (S')^* & 0 \end{bmatrix} \psi' = e^{i\chi} \psi' \quad (10)$$

where $\psi' = \mathcal{U}\psi$, and

$$S' = \mathcal{H}_{2N} e^{-i\hat{\phi}/2} \tilde{S} e^{i\hat{\phi}/2} \mathcal{H}_{2N} = \begin{bmatrix} \mathcal{Z} & i\mathcal{W} \\ -i\mathcal{W} & -\mathcal{Z}^* \end{bmatrix} \quad (11)$$

where $\mathcal{Z} = \sqrt{\mathcal{T}} \cos(\phi/2) - i\sqrt{\mathcal{R}}$ and $\mathcal{W} = \sqrt{\mathcal{T}} \sin(\phi/2)$. Solving the eigenproblem for the electron part of the wavefunction

$$A' \psi'_e = e^{2i\chi} \psi'_e, \quad (12)$$

where

$$A' = S'(S')^* = \begin{bmatrix} \mathcal{A} & -i\mathcal{B} \\ -i\mathcal{B}^* & \mathcal{A} \end{bmatrix}, \quad \mathcal{A} = |\mathcal{Z}|^2 - \mathcal{W}^2, \quad \mathcal{B} = 2\mathcal{Z}\mathcal{W}, \quad (13)$$

we obtain the eigenvalues

$$e^{2i\chi_\pm} = \mathcal{A} \pm i|\mathcal{B}|. \quad (14)$$

From this we compute

$$e^{i\chi_\pm} = \pm \sqrt{\frac{1}{2}(\mathbb{I}_N + \mathcal{A})} + i \sqrt{\frac{1}{2}(\mathbb{I}_N - \mathcal{A})} = \pm|\mathcal{Z}| + i\mathcal{W}, \quad (15)$$

taking into account that for ABSs, the matrix $\text{Im}(e^{i\chi_\pm})$ is positive semi-definite. Energies are proportional to the real part of $e^{i\chi_\pm}$, i.e. $E_\pm = \pm|\Delta\mathcal{Z}| = \pm|\Delta|\sqrt{\mathbb{I}_N - \mathcal{T} \sin^2(\phi/2)}$. The corresponding (electron part) eigenfunctions are

$$\psi'_{e,\pm} = \frac{1}{\sqrt{2}} \begin{bmatrix} \mathcal{Z}/|\mathcal{Z}| \\ \mp \mathbb{I}_N \end{bmatrix} \quad (16)$$

from which the hole part is obtained by $\psi'_{h,\pm} = e^{-i\chi_\pm} (S')^* \psi'_{e,\pm}$, giving the complete set of ABSs:

$$\psi'_\pm = \frac{1}{\sqrt{2}} \begin{bmatrix} \psi'_{e,\pm} \\ \psi'_{h,\pm} \end{bmatrix} = \frac{1}{2} \begin{bmatrix} \mathcal{Z}/|\mathcal{Z}| \\ \mp \mathbb{I}_N \\ \pm \mathbb{I}_N \\ \mathcal{Z}/|\mathcal{Z}| \end{bmatrix}. \quad (17)$$

This can be compactly written in matrix form as

$$[\psi'_+ \ \psi'_-] = [\psi'_a \ \psi'_b] \begin{bmatrix} \mathcal{Z}/|\mathcal{Z}| & 0 \\ 0 & \mathbb{I}_N \end{bmatrix} \mathcal{H}_{2N}, \quad [\psi'_a \ \psi'_b] = \frac{1}{\sqrt{2}} \begin{bmatrix} \mathbb{I}_N & 0 \\ 0 & -\mathbb{I}_N \\ 0 & \mathbb{I}_N \\ \mathbb{I}_N & 0 \end{bmatrix}. \quad (18)$$

We will write the Hamiltonian projected to the subspace of ABSs in terms of the following basis

$$[\psi_\alpha \ \psi_\beta] = \mathcal{U}^\dagger [\psi'_a \ \psi'_b] \mathcal{H}_{2N} e^{i\hat{\phi}/2} = \frac{1}{\sqrt{2}} \begin{bmatrix} 0 & V_1 \\ V_2 & 0 \\ U_1 & 0 \\ 0 & -U_2 \end{bmatrix} \quad (19)$$

which is independent of the superconducting phase ϕ . The projected Hamiltonian is then

$$\begin{aligned} H_p &= \mathcal{U}^\dagger [\psi'_+ \ \psi'_-] \begin{bmatrix} |\Delta\mathcal{Z}| & 0 \\ 0 & -|\Delta\mathcal{Z}| \end{bmatrix} \begin{bmatrix} (\psi'_+)^{\dagger} \\ (\psi'_-)^{\dagger} \end{bmatrix} \mathcal{U} \\ &= |\Delta| [\psi_\alpha \ \psi_\beta] \begin{bmatrix} \text{Re}(\mathcal{Z}) & -ie^{-i\phi/2}\text{Im}(\mathcal{Z}) \\ ie^{i\phi/2}\text{Im}(\mathcal{Z}) & -\text{Re}(\mathcal{Z}) \end{bmatrix} \begin{bmatrix} \psi_\alpha^{\dagger} \\ \psi_\beta^{\dagger} \end{bmatrix} \\ &= |\Delta| [\psi_\alpha \ \psi_\beta] \begin{bmatrix} \sqrt{\mathcal{T}} \cos(\phi/2) & ie^{-i\phi/2}\sqrt{\mathcal{R}} \\ -ie^{i\phi/2}\sqrt{\mathcal{R}} & -\sqrt{\mathcal{T}} \cos(\phi/2) \end{bmatrix} \begin{bmatrix} \psi_\alpha^{\dagger} \\ \psi_\beta^{\dagger} \end{bmatrix} \\ &= |\Theta\rangle \left(\vec{h}_N \cdot (\vec{\Sigma} \otimes \mathbb{I}_N) \right) \langle \Theta| \end{aligned} \quad (20)$$

where in the last step we defined a shortened notation $|\Theta\rangle \equiv [\psi_\alpha \ \psi_\beta]$, $\vec{\Sigma}$ denotes a vector of Pauli matrices acting in the space of states ψ_α and ψ_β , and we defined a $3N$ dimensional analog of a magnetic field:

$$\vec{h}_N = |\Delta| \begin{bmatrix} \sqrt{\mathcal{R}} \sin(\phi/2) \\ -\sqrt{\mathcal{R}} \cos(\phi/2) \\ \sqrt{\mathcal{T}} \cos(\phi/2) \end{bmatrix}. \quad (21)$$

Considering the polar decomposition of the scattering matrix [Eq. (5)], projector $P = |\Theta\rangle\langle\Theta|$ and the projected Hamiltonian H_p can be expressed in terms of reflection and transmission matrices:

$$P = \frac{1}{2} \begin{bmatrix} \mathbb{I}_N & 0 & 0 & -(t't^\dagger)^{-1/2}t' \\ 0 & \mathbb{I}_N & (tt^\dagger)^{-1/2}t & 0 \\ 0 & t^\dagger(tt^\dagger)^{-1/2} & \mathbb{I}_N & 0 \\ -t't^\dagger(t't^\dagger)^{-1/2} & 0 & 0 & \mathbb{I}_N \end{bmatrix}, \quad (22a)$$

$$H_p = \frac{1}{2} \begin{bmatrix} H_e & \mathcal{H} \\ \mathcal{H}^\dagger & H_h \end{bmatrix} = P \begin{bmatrix} 0 & \mathcal{H} \\ \mathcal{H}^\dagger & 0 \end{bmatrix} P, \quad (22b)$$

where

$$H_e = |\Delta| \begin{bmatrix} -\cos(\frac{\phi}{2})(t't^\dagger)^{1/2} & e^{i\phi/2}rt^\dagger(tt^\dagger)^{-1/2} \\ e^{-i\phi/2}(tt^\dagger)^{-1/2}tr^\dagger & \cos(\frac{\phi}{2})(tt^\dagger)^{1/2} \end{bmatrix}, \quad (23a)$$

$$H_h = S^\dagger e^{-i\hat{\phi}} H_e e^{i\hat{\phi}} S = |\Delta| \begin{bmatrix} \cos(\frac{\phi}{2})(t^\dagger t)^{1/2} & e^{-i\phi/2}t^\dagger(tt^\dagger)^{-1/2}r' \\ e^{i\phi/2}r't^\dagger(tt^\dagger)^{-1/2}t & -\cos(\frac{\phi}{2})(t^\dagger t)^{1/2} \end{bmatrix}, \quad (23b)$$

$$\mathcal{H} = \frac{|\Delta|}{2} \{S, e^{i\hat{\phi}}\} = |\Delta| \begin{bmatrix} e^{i\phi/2}r & \cos(\frac{\phi}{2})t' \\ \cos(\frac{\phi}{2})t & e^{-i\phi/2}r' \end{bmatrix}. \quad (23c)$$

This concludes the derivation of the effective Hamiltonian for ABSs. Note that the block H_e is the same as the Hamiltonian shown in Eq. (9) of the main text.

B. Chiral symmetry

The chiral symmetry (CS) [Eq. (6b) of the main text] implies that eigenfunctions come in pairs, where $\Psi(\vec{\alpha}, -\vec{\phi}) = i\tau_y \Psi(\vec{\alpha}, \vec{\phi})$. If we represent the wavefunction $\Psi(\vec{\alpha}, \vec{\phi})$ in the m -th lead in terms of incoming (a_e, a_h) and outgoing (b_e, b_h) waves, we have

$$\Psi(\vec{\alpha}, \vec{\phi}) = \mathcal{N} \begin{bmatrix} e^{-ikx}a_e + e^{ikx}b_e \\ e^{ikx}a_h + e^{-ikx}b_h \end{bmatrix}, \quad (24)$$

where \mathcal{N} is normalization factor, x is the distance from the normal region, and k is the wave vector along x in the m -th lead. Thus, the CS effectively changes (b_e, b_h) to $(a_h, -a_e)$. This translates for the Hamiltonian projected to ABSs [Eq. (20)], which is written in the basis of outgoing waves (as stated in the main text), to

$$H_p(\vec{\alpha}, \vec{\phi}) \begin{bmatrix} b_e \\ b_h \end{bmatrix} = E(\vec{\alpha}, \vec{\phi}) \begin{bmatrix} b_e \\ b_h \end{bmatrix}, \quad (25)$$

$$H_p(\vec{\alpha}, -\vec{\phi}) \begin{bmatrix} a_h \\ -a_e \end{bmatrix} = -E(\vec{\alpha}, \vec{\phi}) \begin{bmatrix} a_h \\ -a_e \end{bmatrix}. \quad (26)$$

Considering the relation between incoming and outgoing waves [4]

$$\begin{bmatrix} a_e \\ a_h \end{bmatrix} = e^{-i\chi} \begin{bmatrix} 0 & e^{i\hat{\phi}} \\ e^{-i\hat{\phi}} & 0 \end{bmatrix} \begin{bmatrix} b_e \\ b_h \end{bmatrix}, \quad (27a)$$

we get

$$\begin{bmatrix} e^{i\hat{\phi}} & 0 \\ 0 & -e^{-i\hat{\phi}} \end{bmatrix} H_p(\vec{\alpha}, -\vec{\phi}) \begin{bmatrix} e^{-i\hat{\phi}} & 0 \\ 0 & -e^{i\hat{\phi}} \end{bmatrix} = -H_p(\vec{\alpha}, \vec{\phi}). \quad (28)$$

In the two-terminal case, for $\phi = 0$ and $\phi = \pi$ we have $\Gamma_0 = \tau_z \otimes \nu_0 \otimes \mathbb{I}_N$ and $\Gamma_\pi = \tau_z \otimes \nu_z \otimes \mathbb{I}_N$, respectively, where ν_0 is 2×2 identity matrix acting in the space of left and right outgoing waves, and ν_z is the Pauli matrix acting in the same space. If we drop the particle-hole degree of freedom and restrict ourselves to only the electron part as we did in the main text, Γ_π becomes $(\nu_z \otimes \mathbb{I}_N)$, as presented in the main text.

Acting with Γ_π on $|\Theta\rangle$, we find that $\Gamma_\pi|\Theta\rangle = -|\Theta\rangle(\Sigma_z \otimes \mathbb{I}_N)$. This demonstrates that at $\phi = \pi$, the states ψ_α and ψ_β are chiral with chirality $-$ and $+$, respectively. In the remainder of this text, we will omit writing \mathbb{I}_N for brevity.

C. Winding number

Proceeding to the computation of the winding number at $\phi = \pi$, we express the flattened Hamiltonian as [1]

$$Q = |\Theta\rangle \left(\hat{h}_N \cdot \vec{\Sigma} \right) \langle \Theta|, \quad (29)$$

where $\hat{h}_N = \vec{h}_N / |\vec{h}_N| = [1, 0, 0]^T$.

Let us first compute $\langle \Theta|\Theta\rangle$ and $\langle \Theta|d\Theta\rangle$:

$$\langle \Theta|\Theta\rangle = \begin{bmatrix} \psi_\alpha^\dagger \psi_\alpha & 0 \\ 0 & \psi_\beta^\dagger \psi_\beta \end{bmatrix} = \begin{bmatrix} \mathbb{I}_N & 0 \\ 0 & \mathbb{I}_N \end{bmatrix}, \quad (30a)$$

$$\langle \Theta|d\Theta\rangle = \begin{bmatrix} \psi_\alpha^\dagger d\psi_\alpha & 0 \\ 0 & \psi_\beta^\dagger d\psi_\beta \end{bmatrix} = \frac{1}{2} \begin{bmatrix} V_2^\dagger dV_2 + U_1^\dagger dU_1 & 0 \\ 0 & V_1^\dagger dV_1 + U_2^\dagger dU_2 \end{bmatrix}. \quad (30b)$$

Now we evaluate the winding number:

$$\begin{aligned} W_\pi &= \frac{1}{4\pi i} \oint_{\mathcal{C}_\alpha} \text{tr}_p [\Gamma_\pi Q dQ] \\ &= \frac{1}{4\pi i} \oint_{\mathcal{C}_\alpha} \text{tr}_p [|\Theta\rangle (-\Sigma_z) \Sigma_x \langle \Theta| dQ] \\ &= \frac{1}{4\pi i} \oint_{\mathcal{C}_\alpha} \text{tr} [-\Sigma_y \langle \Theta| d(|\Theta\rangle \Sigma_x \langle \Theta|) |\Theta\rangle] \\ &= \frac{1}{2\pi i} \oint_{\mathcal{C}_\alpha} \text{tr} [-\Sigma_z \langle \Theta| d|\Theta\rangle] \\ &= \frac{1}{4\pi i} \oint_{\mathcal{C}_\alpha} \text{tr} [V_1^\dagger dV_1 + U_2^\dagger dU_2 - V_2^\dagger dV_2 - U_1^\dagger dU_1], \end{aligned} \quad (31)$$

where \mathcal{C}_α denotes a connected path in the space of AC fluxes $\vec{\alpha} = [\alpha_1, \alpha_2]^T$, tr_p indicates tracing over all ABSs, and tr is the trace of a matrix. Considering the polar decomposition of r and r' , the above expression can be rewritten as

$$W_\pi = \frac{1}{4\pi i} \oint_{\mathcal{C}_\alpha} \text{tr} [r^{-1} dr - (r')^{-1} dr'] = \frac{1}{2} (W_r - W_{r'}) \quad (32)$$

where we define the winding numbers W_r and $W_{r'}$ for the reflection matrices r and r' , respectively.

From $\det(r^\dagger r'^\dagger) = -\det(\mathcal{RT})$, we derive the relation

$$W_r + W_{r'} = W_t + W_{t'}, \quad (33)$$

where in the derivation, we assume that \mathcal{R} and \mathcal{T} are not singular anywhere on the path \mathcal{C}_α , ensuring that derivatives and winding numbers are well-defined. If the path \mathcal{C}_α does not enclose any singularities in t or t' , i.e. no gap touching singularities, then $W_r + W_{r'} = W_t + W_{t'} = 0$. Thus, we obtain the result for the winding number at $\phi = \pi$:

$$W_\pi = W_r = \frac{1}{2\pi i} \oint_{\mathcal{C}_\alpha} \text{tr} [r^{-1} dr] = \frac{1}{2\pi i} \oint_{\mathcal{C}_\alpha} d \log [\det(r)] \quad (34)$$

which is the same as the one presented in the main text under the same assumptions.

D. Low-energy Hamiltonian

Let us derive the low-energy Hamiltonian near the Weyl node at \vec{x}_w . At \vec{x}_w , we choose for the basis the two chiral states crossing at the Weyl node (indicated by subscript 0), denoted as $|a^- \rangle \equiv |\psi_{\alpha,0}(\vec{x}_w)\rangle$ and $|a^+ \rangle \equiv |\psi_{\beta,0}(\vec{x}_w)\rangle$ (note the computation of chiralities of $\psi_{\alpha,\beta}$ at the end of the previous subsection). Additionally, $H_p(\vec{x}_w)|a^\pm \rangle = 0$. Expressing the eigenfunctions at \vec{x} , where $|\vec{x} - \vec{x}_w| \ll 1$, in terms of this basis, we have:

$$|\psi_0^\pm(\vec{x})\rangle \approx \alpha^\pm |a^+\rangle + \beta^\pm |a^-\rangle. \quad (35)$$

From here, we obtain

$$H_p(\vec{x})|\psi_0^\pm(\vec{x})\rangle \approx (H_p(\vec{x}_w) + \delta\vec{x} \cdot \nabla_{\vec{x}} H_p(\vec{x}_w)) (\alpha^\pm |a^+\rangle + \beta^\pm |a^-\rangle) = E_0^\pm(\vec{x}) (\alpha^\pm |a^+\rangle + \beta^\pm |a^-\rangle) \quad (36)$$

where $\delta\vec{x} = \vec{x} - \vec{x}_w$. Projecting this onto the states $|a^\pm \rangle$, we obtain a linear system:

$$\begin{bmatrix} \langle a^+ | \\ \langle a^- | \end{bmatrix} (\delta\vec{x} \cdot \nabla_{\vec{x}} H_p(\vec{x}_w)) \begin{bmatrix} |a^+\rangle \\ |a^-\rangle \end{bmatrix} \begin{bmatrix} \alpha^\pm \\ \beta^\pm \end{bmatrix} = E_0^\pm(\vec{x}) \begin{bmatrix} \alpha^\pm \\ \beta^\pm \end{bmatrix}. \quad (37)$$

From this, we can derive the Weyl Hamiltonian in the basis of chiral states $|a^\pm \rangle$:

$$H_W = \delta\vec{x} \cdot M_3 \vec{\Sigma} \quad (38)$$

where

$$M_3 \vec{\Sigma} = \begin{bmatrix} \langle a^+ | \\ \langle a^- | \end{bmatrix} (\nabla_{\vec{x}} H_p(\vec{x}_w)) \begin{bmatrix} |a^+\rangle \\ |a^-\rangle \end{bmatrix}. \quad (39)$$

Now, let us evaluate the matrix M_3 row by row. Starting with α_i , we have:

$$(M_3)_{[\alpha_i \bullet]} \vec{\Sigma} = \begin{bmatrix} \langle a^+ | \\ \langle a^- | \end{bmatrix} (\partial_{\alpha_i} H_p(\vec{x}))|_{\vec{x}=\vec{x}_w} \begin{bmatrix} |a^+\rangle \\ |a^-\rangle \end{bmatrix} \quad (40a)$$

$$= \partial_{\alpha_i} \left(\begin{bmatrix} \langle a^+ | \\ \langle a^- | \end{bmatrix} |\Theta(\vec{\alpha})\rangle \left(\Sigma_x \otimes \sqrt{\mathcal{R}(\vec{\alpha})} \right) \langle \Theta(\vec{\alpha}) | \begin{bmatrix} |a^+\rangle \\ |a^-\rangle \end{bmatrix} \right) \Big|_{\vec{\alpha}=\vec{\alpha}_w} \quad (40b)$$

$$\approx \partial_{\alpha_i} \left(\begin{bmatrix} 0 & \langle a^+ | \psi_{\beta,0}(\vec{\alpha}) \rangle \\ \langle a^- | \psi_{\alpha,0}(\vec{\alpha}) \rangle & 0 \end{bmatrix} \begin{bmatrix} 0 & \sqrt{\mathcal{R}_0(\vec{\alpha})} \\ \sqrt{\mathcal{R}_0(\vec{\alpha})} & 0 \end{bmatrix} \begin{bmatrix} 0 & \langle \psi_{\alpha,0}(\vec{\alpha}) | a^- \rangle \\ \langle \psi_{\beta,0}(\vec{\alpha}) | a^+ \rangle & 0 \end{bmatrix} \right) \Big|_{\vec{\alpha}=\vec{\alpha}_w} \quad (40c)$$

$$= \begin{bmatrix} 0 & \partial_{\alpha_i} \tilde{\zeta}(\vec{\alpha}_w) \\ \partial_{\alpha_i} \tilde{\zeta}^*(\vec{\alpha}_w) & 0 \end{bmatrix} = \text{Re}(\partial_{\alpha_i} \tilde{\zeta}(\vec{\alpha}_w)) \Sigma_x - \text{Im}(\partial_{\alpha_i} \tilde{\zeta}(\vec{\alpha}_w)) \Sigma_y, \quad (40d)$$

where \mathcal{R}_0 is the smallest singular value of rr^\dagger , and $\tilde{\zeta}(\vec{\alpha}) = \langle a^+ | \psi_{\beta,0}(\vec{\alpha}) \rangle \sqrt{\mathcal{R}_0(\vec{\alpha})} \langle \psi_{\alpha,0}(\vec{\alpha}) | a^- \rangle$ is a complex scalar. Similarly, for ϕ , we have:

$$\begin{aligned} (M_3)_{[\phi \bullet]} \vec{\Sigma} &= \begin{bmatrix} \langle a^+ | \\ \langle a^- | \end{bmatrix} (\partial_\phi H_p(\vec{x}))|_{\vec{x}=\vec{x}_w} \begin{bmatrix} |a^+\rangle \\ |a^-\rangle \end{bmatrix} \\ &\approx \partial_\phi \left(\begin{bmatrix} 0 & \langle a^+ | \psi_{\beta,0}(\vec{\alpha}_w) \rangle \\ \langle a^- | \psi_{\alpha,0}(\vec{\alpha}_w) \rangle & 0 \end{bmatrix} \begin{bmatrix} \cos(\phi/2) & 0 \\ 0 & -\cos(\phi/2) \end{bmatrix} \begin{bmatrix} 0 & \langle \psi_{\alpha,0}(\vec{\alpha}_w) | a^- \rangle \\ \langle \psi_{\beta,0}(\vec{\alpha}_w) | a^+ \rangle & 0 \end{bmatrix} \right) \Big|_{\phi=\pi} \\ &= \Sigma_x \left(-\frac{1}{2} \Sigma_z \right) \Sigma_x = \frac{1}{2} \Sigma_z. \end{aligned} \quad (41)$$

Thus, the matrix M_3 can be written in the same form as in the main text

$$M_3 = \begin{bmatrix} M_2 & 0 \\ 0 & 0 \end{bmatrix}, \quad M_2 = \begin{bmatrix} \partial_{\alpha_1} \text{Re}(\tilde{\zeta}) & -\partial_{\alpha_1} \text{Im}(\tilde{\zeta}) \\ \partial_{\alpha_2} \text{Re}(\tilde{\zeta}) & -\partial_{\alpha_2} \text{Im}(\tilde{\zeta}) \end{bmatrix}_{\vec{\alpha}=\vec{\alpha}_W}, \quad (42)$$

although with $\tilde{\zeta}$ replacing ζ of the main text. Still, the same argument that $W_W = \text{sgn}(\det(M_2)) = \text{sgn}(\det(M_3)) = C_W$ can be made. This also demonstrates the dispersion is conical at \vec{x}_W with the low-energy dispersion being

$$E_0^\pm(\delta\vec{x}) = \pm \sqrt{|\delta\vec{\alpha} \cdot \nabla_{\vec{\alpha}} \tilde{\zeta}|^2 + \left(\frac{\delta\phi}{2}\right)^2}. \quad (43)$$

Let us now demonstrate the connection between $\tilde{\zeta}$ and ζ of the main text. Equation (40a) can be expressed as

$$\partial_{\alpha_i} \left(\frac{1}{2} \begin{bmatrix} \langle a_e^+ | & \langle a_h^+ | \\ \langle a_e^- | & \langle a_h^- | \end{bmatrix} H_p(\vec{\alpha}, \phi = \pi) \begin{bmatrix} |a_e^+\rangle & |a_e^-\rangle \\ |a_h^+\rangle & |a_h^-\rangle \end{bmatrix} \right) \Big|_{\vec{\alpha}=\vec{\alpha}_W} \quad (44)$$

with $|a_{e,h}^\pm\rangle$ being the electron and hole parts of $|a^\pm\rangle$, which leads to an alternative expression for $\tilde{\zeta}$:

$$\tilde{\zeta} = \frac{1}{4} (\langle a_e^+ | H_e | a_e^- \rangle + \langle a_e^+ | \mathcal{H} | a_h^- \rangle + \langle a_h^+ | \mathcal{H}^\dagger | a_e^- \rangle + \langle a_h^+ | H_h | a_h^- \rangle), \quad (45)$$

where the first (electronic) term is the same as in the main text, being equal to ζ . However, as we have shown in the previous subsection, working with the full states or just with their electronic parts yields the same topological charges. Hence, while performing the full computation involving both electron and hole parts introduces additional terms in $\tilde{\zeta}$ compared to the approach outlined in the main text, this adjustment does not alter any of the conclusions regarding the system's topology.

-
- [1] K. Shiozaki and M. Sato, [Phys. Rev. B **90**, 165114 \(2014\)](#).
 - [2] T. Martin and R. Landauer, [Phys. Rev. B **45**, 1742 \(1992\)](#).
 - [3] C. W. J. Beenakker, [Rev. Mod. Phys. **69**, 731 \(1997\)](#).
 - [4] C. W. J. Beenakker, [Phys. Rev. Lett. **67**, 3836 \(1991\)](#).